

As the rotation rate of the degenerate core is reduced by magnetic braking and the convective envelope is removed, the stellar dynamo will shut down. Some remnant field anchored in the core will survive even without a convection zone, although the convective envelope may not be removed completely. Indeed, white dwarfs do have thin surface convection zones which can support a near-surface dynamo in the white dwarf itself²⁰.

We have thus demonstrated that dynamos are likely to operate in AGB stars. As a star evolves off the AGB, the dynamo-generated magnetic field will be strong enough to drive a strong, self-collimating outflow and to slow the rotation of the core by magnetic braking. Eruptions analogous to coronal mass ejections, expected as a consequence of the dynamo activity, could produce asymmetric structures in the wind. Thus our model opens up the possibility of constructing a new, self-consistent paradigm for planetary-nebula formation, beginning with AGB stars and ending with slowly rotating white dwarfs. □

Received 10 August; accepted 28 November 2000.

1. Kwok, S., Purton, C. R. & Fitzgerald, P. M. On the origin of planetary nebulae. *Astrophys. J.* **219**, L125–L127 (1978).
2. Manchado, A., Villaver, E., Stanghellini, L. & Guerrero, M. in *Asymmetrical Planetary Nebulae II. From Origins to Microstructures* (eds Kastner, J. H., Stoker, N. & Rappaport, S.) 17–23 (ASP Conf. Ser. 199, Astronomical Society of the Pacific, San Francisco, 2000).
3. Soker, N. & Harpaz, A. Can a single AGB star form an axially symmetric planetary nebula? *J. Astron. Soc. Pac.* **104**, 923–930 (1992).
4. Koester, D., Dreizler, S., Weidemann, V. & Allard, N. F. Search for rotation in white dwarfs. *Astron. Astrophys.* **338**, 612–622 (1998).
5. Balick, B. The evolution of planetary nebulae. I—Structures, ionizations, and morphological sequences. *Astron. J.* **94**, 671–678 (1987).
6. Soker, N. & Livio, M. Interacting winds and the shaping of planetary nebulae. *Astrophys. J.* **339**, 268–278 (1989).
7. Mellema, G., Eulderink, F. & Icke, V. Hydrodynamical models of aspherical planetary nebulae. *Astron. Astrophys.* **252**, 718–732 (1991).
8. Icke, V., Balick, B. & Frank, A. The hydrodynamics of aspherical planetary nebulae. II. Numerical modelling of the early evolution. *Astron. Astrophys.* **253**, 224–243 (1992).
9. Gurzadyan, G. *Planetary Nebulae* (Gordon and Breach, New York, 1969).
10. Pascoli, G. La nature des nébuleuses planétaires bipolaires. *Astron. Astrophys.* **180**, 191–200 (1987).
11. Matt, S., Balick, B., Winglee, R. & Goodson, A. Disk formation by asymptotic giant branch winds in dipole magnetic fields. *Astrophys. J.* **545**, 965–973 (2000).
12. Chevalier, R. A. & Luo, D. Magnetic shaping of planetary nebulae and other stellar wind bubbles. *Astrophys. J.* **421**, 225–235 (1994).
13. García-Segura, G., Langer, N., Rozyczka, M. & Franco, J. Shaping bipolar and elliptical planetary nebulae: effects of stellar rotation, photoionization beating, and magnetic fields. *Astrophys. J.* **517**, 767–781 (1999).
14. Blackman, E. G., Frank, A. & Welch, C. MHD stellar and disk winds: Application to planetary nebulae. *Astrophys. J.* (in the press).
15. Cox, A. N. *Allen's Astrophysical Quantities* 4th edn, 389 (AIP Press, New York, 1999).
16. Peterson, R. C. The rotation of horizontal-branch stars. II. Members of the globular clusters M3, M5, and M13. *Astrophys. J.* **275**, 737–751 (1983).
17. Pinsonneault, M., Deliyannis, C. P. & Demarque, P. Evolutionary models of halo stars with rotation. I. Evidence for differential rotation with depth in stars. *Astrophys. J.* **367**, 239–252 (1991).
18. Behr, B. B. *et al.* A new spin on the problem of horizontal-branch gaps: stellar rotation along the blue horizontal branch of globular cluster M13. *Astrophys. J.* **528**, 849–853 (2000).
19. Livio, M. & Pringle, J. E. The rotation rates of white dwarfs and pulsars. *Astrophys. J.* **505**, 339–343 (1998).
20. Thomas, J. H., Markiel, J. A. & Van Horn, H. M. Dynamo generation of magnetic fields in white dwarfs. *Astrophys. J.* **453**, 403–410 (1995).
21. Parker, E. N. A solar dynamo surface wave at the interface between convection and nonuniform rotation. *Astrophys. J.* **408**, 707–719 (1993).
22. Markiel, J. A. & Thomas, J. H. Solar interface dynamo models with a realistic rotation profile. *Astrophys. J.* **523**, 827–837 (1999).
23. Blackman, E. G. Overcoming the back reaction on turbulent motions in the presence of magnetic fields. *Phys. Rev. Lett.* **77**, 2694–2697 (1996).
24. Pick, M. in *Ninth European Meeting on Solar Physics: Magnetic Fields and Solar Processes* (ed. Wilson, A.) 183 (ESA SP Series SP-448, European Space Agency, 1999).
25. Trammell, S. R. in *Asymmetrical Planetary Nebulae II. From Origins to Microstructures* (eds Kastner, J. H., Soker, N. & Rappaport, S.) 147–150 (ASP Conf. Ser. 199, Astronomical Society of the Pacific, San Francisco, 2000).
26. Sahai, J. in *Asymmetrical Planetary Nebulae II. From origins to Microstructures* (eds Kastner, J. H., Soker, N. & Rappaport, S.) 209–216 (ASP Conf. Ser. 199, Astronomical Society of the Pacific, San Francisco, 2000).
27. Alcolea, J. *et al.* in *Asymmetrical Planetary Nebulae II. From Origins to Microstructures* (eds Kastner, J. H., Soker, N. & Rappaport, S.) 347–354 (ASP Conf. Ser. 199, Astronomical Society of the Pacific, San Francisco, 2000).
28. König, A. & Pudritz, R. in *Protostars and Planets IV* (eds Mannings, V., Boss, V. A. & Russell, S.) 759–791 (Univ. Arizona Press, Tucson, 2000).
29. Tsiganos, K. & Bogovalov, S. Magnetic collimation of solar and stellar winds. *Astron. Astrophys.* **356**, 989–1002 (2000).

30. Lery, T., Heyvaerts, J., Appl, S. & Norman, C. Outflows from magnetic rotators. *Astron. Astrophys.* **337**, 603–624 (1998).
31. Balick, B. *et al.* FLIERs and other microstructures in planetary nebulae. IV. Images of elliptical PNs from the Hubble Space Telescope. *Astron. J.* **116**, 360–371 (1999).
32. Palen, S. & Fix, J. D. Models of OH maser variations in U Herculis. *Astrophys. J.* **531**, 391–400 (2000).

Acknowledgements

We are grateful to S. Kawaler and to F. D'Antona and P. Ventura for making available to us detailed tables of their evolutionary models for AGB stars. This work was supported by the NSF, NASA and the DOE.

Correspondence and requests for materials should be addressed to J.H.T. (e-mail: thomas@astro.me.rochester.edu).

.....
Geochemical evidence for magmatic water within Mars from pyroxenes in the Shergotty meteorite

Harry Y. McSween Jr^{*}, Timothy L. Grove[†], Rachel C. F. Lentz^{*}, Jesse C. Dann[‡], Astrid H. Holzheid[‡], Lee R. Ricuputi[‡] & Jeffrey G. Ryan[§]

^{*} Department of Geological Sciences, University of Tennessee, Knoxville, Tennessee 37996, USA

[†] Department of Earth, Atmospheric and Planetary Sciences, Massachusetts Institute of Technology, Cambridge, Massachusetts 02139, USA

[‡] Chemical and Analytical Sciences Division, Oak Ridge National Laboratory, Oak Ridge, Tennessee 37831, USA

[§] Department of Geology, University of South Florida, Tampa, Florida 33620, USA

.....
Observations of martian surface morphology have been used to argue that an ancient ocean once existed on Mars¹. It has been thought that significant quantities of such water could have been supplied to the martian surface through volcanic outgassing, but this suggestion is contradicted by the low magmatic water content that is generally inferred from chemical analyses of igneous martian meteorites². Here, however, we report the distributions of trace elements within pyroxenes of the Shergotty meteorite—a basalt body ejected 175 million years ago from Mars³—as well as hydrous and anhydrous crystallization experiments that, together, imply that water contents of pre-eruptive magma on Mars could have been up to 1.8%. We found that in the Shergotty meteorite, the inner cores of pyroxene minerals (which formed at depth in the martian crust) are enriched in soluble trace elements when compared to the outer rims (which crystallized on or near to the martian surface). This implies that water was present in pyroxenes at depth but was largely lost as pyroxenes were carried to the surface during magma ascent. We conclude that ascending magmas possibly delivered significant quantities of water to the martian surface in recent times, reconciling geologic and petrologic constraints on the outgassing history of Mars.

The Shergotty meteorite is a martian basalt (shergottite), approximately 175 million years old³, with measured water contents⁴ of only 130–350 parts per million (p.p.m.). Pyroxenes (pigeonite and augite) were the earliest crystallizing minerals, and the homogeneous magnesian cores of these grains are thought to have formed at depth and been entrained in the ascending magma^{3,5}. During ascent or eruption, the pyroxenes developed iron-rich rims, as plagioclase and other minerals joined the crystallization sequence. The pyroxene core and rim compositions thus reflect magma compositions at depth and near (or on) the planet's surface,

respectively. The presence of hydrous amphibole within trapped melt inclusions in pyroxene cores previously fuelled speculation that the Shergotty magma contained 1–2 wt% water at depth⁶, but conflicting interpretations of the low measured hydrogen contents in these amphiboles^{7–9} suggest that this evidence is inconclusive.

Abundances of trace elements in cores and rims also record the magma's evolution. Analyses of Li, Be, B, Ce, Y and Ti in Shergotty pyroxenes using secondary-ion mass spectrometry are summarized in Table 1 of Supplementary Information. During fractional crystallization of pyroxenes, all these incompatible elements should partition into the melt, and thus their abundances should increase from pyroxene cores to rims. As expected, Be and Ti increase from core to rim, whereas B and Li decrease (Fig. 1a, b). Ce also appears to decrease relative to Y, which behaves similarly to heavy rare-earth elements (Fig. 1c).

The presence of hot aqueous fluid could alter the expected partitioning behaviour during fractional crystallization, because B and Li are soluble at temperatures greater than 350 °C (ref. 10). Partitioning of these elements between clinopyroxene, magma and fluids has been studied experimentally at magmatic temperatures¹¹, revealing clear preferences for the aqueous phase. Unlike most other rare-earth elements, cerium can exist in more than one valence state, but any Ce⁴⁺ in magma should be reduced by Fe²⁺. Ce³⁺ has been suggested to be more soluble than other rare earths, possibly accounting for negative Ce anomalies observed in some subduction-zone lavas¹². Thus Ce might also partition into an aqueous fluid, although its concentration in pyroxene rims might also be affected if whitlockite co-crystallized. The observed depletions of B, Li, and perhaps Ce/Y in Shergotty pyroxene rims are

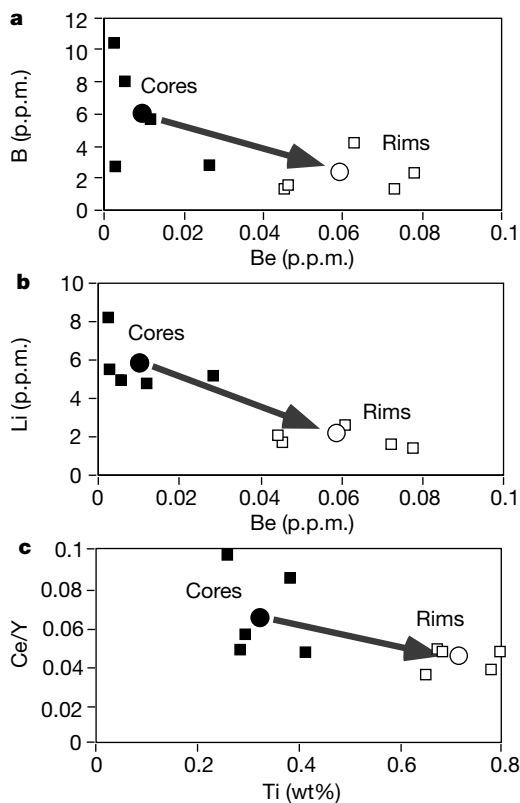


Figure 1 Measured abundances of B (a) and Li (b), and the measured Ce/Y ratio (c), relative to other incompatible elements (Be and Ti), in Shergotty pyroxenes. We interpret decreases in B, Li and Ce/Y from cores (filled symbols) to rims (open symbols) to reflect loss of soluble trace elements in an exsolved aqueous fluid. Analytical uncertainties for individual analyses (squares) are within the sizes of the points, and average values are indicated by circles.

consistent with removal of aqueous fluid after crystallization of the cores at depth. These observations suggest that water, carrying soluble trace elements, was exsolved and lost from the magma on ascent and eruption.

The Mg/(Mg+Fe) ratios of pigeonite and augite cores indicate that both pyroxenes in Shergotty crystallized simultaneously^{5,13}. Imaging shows that Shergotty contains approximately 13 vol.% of accumulated pyroxene cores, and the composition of crystal-free liquid has been estimated by subtracting pyroxenes from the bulk meteorite composition¹³. We performed crystallization experiments on this intercumulus liquid composition to determine if it would co-crystallize augite and pigeonite with compositions like those in Shergotty. Initial experimental conditions were anhydrous, at a pressure of 0.1 MPa and an oxygen fugacity set by the quartz–fayalite–magnetite (QFM) buffer. Compositions of pyroxenes crystallized under these conditions are summarized in Fig. 2. The Shergotty liquid composition did not produce a crystallizing assemblage at 0.1 MPa resembling the mineral assemblage in Shergotty. Instead of augite and pigeonite coexisting as liquidus phases, our 0.1-MPa results show a large crystallization interval for pigeonite (~100 °C) before an Fe-enriched low-wollastonite (low-Wo) augite appears (Fig. 2). Similar experimental results have been documented by other workers^{14,15}. Calculations of the crystallization sequence at elevated pressures¹³ and crystallization experiments undertaken at varying oxygen fugacities¹⁵ indicate that this discrepancy is not an effect of increased pressure or a different oxidation state.

We performed a second series of experiments at elevated water pressures (100 and 200 MPa) to test the influence of H₂O on the Shergotty crystallization sequence. At 100 MPa pigeonite was again the liquidus phase, and crystallized over a significant temperature interval (~80 °C) before augite appeared. The effect of the elevated H₂O content of the 200-MPa experiment was to expand the olivine primary phase volume so that the Shergotty intercumulus liquid was saturated near its liquidus with olivine, pigeonite and augite. Because the pigeonite and augite coexist as near-liquidus phases, pyroxenes from the 200-MPa experiments are very similar to the Shergotty pyroxene cores (Fig. 2). However, the CaSiO₃ (Wo) contents of the pigeonite cores in Shergotty are higher by ~4 mol% (average Wo content, 13 mol%) than that produced in the 200-MPa experiment (average Wo, 8.7 mol%) (see Table 2 of Supplementary Information). The difference in Wo content implies that pigeonite and augite in the Shergotty meteorite crystallized at

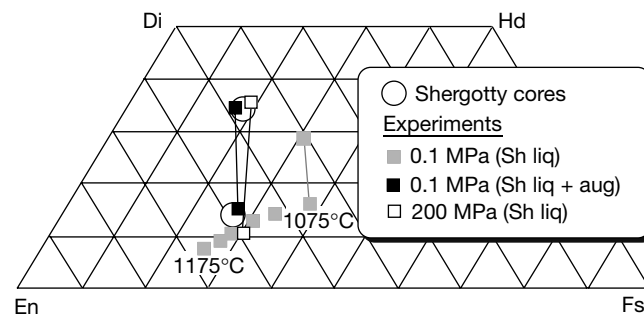


Figure 2 Comparison of the average compositions of Shergotty pigeonite and augite cores with experimental pyroxenes. The figure shows compositions of pyroxenes from anhydrous 0.1-MPa and water-saturated 200-MPa experiments, using the Shergotty liquid composition estimated in ref. 14 and a second composition which is an 85:15 mixture of this liquid and clinopyroxene (2 hedenbergite: 1 salite) with the same Mg/(Mg+Fe) ratio. Vertical bars connect the compositions of the first crystallizing coexisting pyroxenes. En, enstatite MgSiO₃; Fs, ferrosilite FeSiO₃; Di, diopside CaMgSi₂O₆; Hd, hedenburgite CaFeSi₂O₆; Sh liq, Shergotty intercumulus liquid; Sh liq+aug, Sh liq with augite added.

higher temperature than in our 200-MPa experiment. The effect of H₂O is to bring pigeonite and augite nearer the liquidus, but the 200-MPa experimental pyroxenes are not identical to the Shergotty pigeonite and augite cores.

To produce a melt saturated with two pyroxenes on its liquidus at lower water contents, the bulk composition must be modified slightly. We synthesized a new liquid composition by adding 15 wt% augite that had an Mg/(Mg+Fe) ratio similar to that of the intercumulus liquid. This modified composition was run at 0.1 and 100 MPa. At 100 MPa, augite and pigeonite are liquidus phases at 1,150 °C. At 0.1 MPa, augite is the liquidus phase at 1,170 °C, and both augite and pigeonite are present at 1,150 °C at the QFM buffer. The average pigeonite composition in the 0.1-MPa run has 14.7 mol% Wo (Fig. 2). Therefore, the composition of the liquidus pigeonite and augite in Shergotty records a temperature and H₂O content that is between our 0.1-MPa anhydrous result and the hydrous 100- and 200-MPa experiments.

The effect of variations in temperature on the compositions of coexisting augite and pigeonite has been investigated previously¹⁶. The reported relation between temperature and the Wo content of pigeonite coexisting with augite on the pigeonite–augite solvus is identical to that obtained in the present work from the 0.1-MPa and 200-MPa Shergotty experiments. Therefore, the conditions of crystallization of the Shergotty pyroxenes can be used to infer the liquidus temperature and pre-eruptive H₂O pressure. The effects of variations in H₂O pressure on the temperature of the vapour-saturated liquidus are well known for natural basaltic magmas^{17,18}. Using the 0.1- and 200-MPa pigeonites that coexist with augite as a guide, we estimated by interpolation the liquidus temperature for augite and pigeonite in the Shergotty meteorite. We obtained a temperature of 1,120 °C and a magmatic H₂O content of ~1.8 wt%. These pre-eruptive conditions correspond to a pressure of ~55 MPa

using the model of ref. 19, or a depth of ~5 km in the martian crust. This pre-eruptive H₂O content is similar to the dissolved water content inferred for other martian magmas²⁰, and also to the composition of andesitic rocks determined by the Mars Pathfinder²¹.

The magmatic evolution of the Shergotty parent magma that we propose is illustrated in Fig. 3. Vesiculation and loss of water occurred after pyroxene cores crystallized at a depth of greater than 5 km. Although no vesicles are observed in Shergotty, a model of volatile exsolution in martian magmas²² indicates that outgassing should be gradual but continuous above this depth. Because of lower martian gravity, gas exsolution begins at greater depth than on Earth, and the low atmospheric pressure on Mars encourages thorough degassing as the magma ascends²³. Magma outgassing, even on Earth, can be very efficient; for example, viscous rhyolitic magma at Mono Craters, California, was found to lose more than 95% of its total water—from 2.4 to 0.11 wt%—on ascent²⁴.

Can we generalize the Shergotty meteorite results to Mars? Based on similarities in visible and near-infrared reflectance spectra, Shergotty-like basalts have been suggested to dominate large areas of the martian surface²⁵, although basalts mapped by thermal emission spectroscopy on the Mars Global Surveyor orbiter²⁶ appear to have spectra distinct from shergottites.

Although the water content of the Shergotty magma may have increased during fractionation before the crystallization of pyroxene phenocrysts, the presence of ~1.8 wt% water appears to be inconsistent with the dry mantle of the conventional Mars model². This model² estimates the abundance of water in the martian mantle to be 36 p.p.m., on the basis of the abundance of Cl and the relative solubilities of Cl and H₂O in basaltic magma. The same procedure would give an incorrect estimation of water in the Earth's mantle, because Cl has been sequestered in the crust. A newer Mars compositional model²⁷, based on matching oxygen isotopes, suggests a bulk-planet Cl abundance eight times higher than that estimated from element ratios, which would imply a correspondingly greater mantle water content. A value of several hundred p.p.m. of water is comparable to the terrestrial mantle; it is also consistent with observed enrichments of other volatile elements in martian meteorites², and allows higher magmatic water contents at reasonable degrees of partial melting. Alternatively, a Shergotty magma produced by anhydrous mantle melting could have interacted with metasomatized, hydrated mantle lithosphere during ascent.

It is also possible that the water in the Shergotty meteorite was added during assimilation of martian crustal materials or by interaction with martian groundwater systems²¹. Trace-element and radiogenic-isotope patterns in Shergotty have been interpreted to reflect contamination by the martian crust^{28,29}, and the high oxidation state of Shergotty relative to some other shergottites³⁰ suggests that the assimilate may have been at least partly fluid. In any case, the inference that outgassing occurred in martian basaltic magma that erupted relatively recently (~175 Myr ago) argues that substantial water must have been delivered by magmas to the planet's surface in middle martian history. □

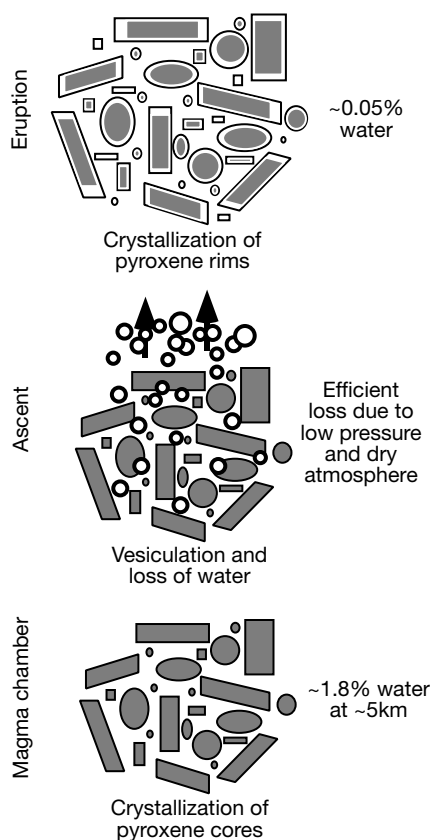


Figure 3 Schematic illustration of pyroxene crystallization and outgassing of the Shergotty parent magma at depth, during ascent, and on eruption.

Methods

Shergotty USNM 321-2 was soaked for 2 h in a 1% mannitol solution, and rinsed in B-free distilled water to minimize surface contamination by B. The section was promptly coated with Au and analysed using the Oak Ridge National Laboratory Cameca ims-4f ion probe. The sample was bombarded with a 12.5-kV primary beam of ¹⁶O⁻ ions, using a primary beam current of 10 nA and a beam size of ~20 μm. Positive secondary ions were extracted into the secondary mass spectrometer with a mass resolution of ~600 to eliminate the interference of Al³⁺ on ⁹Be. An energy offset of 80 eV was applied to eliminate molecular ions. Calibration curves were derived using multiple measurements of natural mineral and glass standards. Detection limits for Li, Be, B, Ce, Y and Ti were well below measured values.

The crystallization temperatures of pigeonite and augite in Shergotty were estimated using the pyroxenes in the experiment of longest duration. The 0.1-MPa experiment was run for 168 h and the 200-MPa experiment was run for 26 h under hydrous conditions.

These experimental durations produced relatively homogeneous crystalline products, as determined by electron microprobe. The 100-MPa experiment is at extreme conditions for hydrous experiments and could only be run for 9 h. The compositions of these pyroxenes varied significantly and were not used to estimate crystallization temperature.

Received 8 August; accepted 20 November 2000.

1. Head, J. W. *et al.* Possible ancient oceans on Mars: Evidence from Mars Orbiter laser altimeter data. *Science* **286**, 2134–2137 (1999).
2. Waenke, H. & Dreibus, G. Chemistry and accretion history of Mars. *Phil. Trans. R. Soc. Lond. A* **349**, 285–293 (1994).
3. McSween, H. Y. Jr What we have learned about Mars from SNC meteorites. *Meteoritics* **29**, 757–779 (1994).
4. Karlsson, H. R., Clayton, R. N., Gibson, E. K. Jr & Mayeda, T. K. Water in SNC meteorites: Evidence for a martian hydrosphere. *Science* **255**, 1409–1411 (1992).
5. Stolper, E. M. & McSween, H. Y. Jr Petrology and origin of the shergottite meteorites. *Geochim. Cosmochim. Acta* **43**, 1475–1498 (1979).
6. McSween, H. Y. Jr & Harvey, R. P. Outgassed water on Mars: Constraints from melt inclusions in SNC meteorites. *Science* **259**, 1890–1892 (1993).
7. Watson, L. L., Hutcheon, I. D., Epstein, S. & Stolper, E. M. Water on Mars: Clues from deuterium/hydrogen and water contents of hydrous phases in SNC meteorites. *Science* **265**, 86–90 (1994).
8. Mysen, B. O., Virgo, D., Popp, R. K. & Bertka, C. M. The role of H₂O in martian magmatic systems. *Am. Mineral.* **83**, 942–946 (1998).
9. King, P. L., Hervig, R. L., Holloway, J. R., Vennemann, T. W. & Righter, K. Oxy-substitution and dehydrogenation in mantle-derived amphibole megacrysts. *Geochim. Cosmochim. Acta* **63**, 3635–3651 (1999).
10. Seyfried, W. E. Jr, Janeky, D. R. & Mottl, M. J. Alteration of the oceanic crust: implications for geochemical cycles of lithium and boron. *Geochim. Cosmochim. Acta* **48**, 557–569 (1984).
11. Brennan, J. M., Ryerson, F. J. & Shaw, H. F. The role of aqueous fluids in the slab-to-mantle transfer of boron, beryllium, and lithium during subduction: Experiments and models. *Geochim. Cosmochim. Acta* **62**, 33337–3347 (1998).
12. Neal, C. R. & Taylor, L. A. A negative Ce anomaly in a peridotite xenolith: Evidence for crustal recycling into the mantle or mantle metasomatism? *Geochim. Cosmochim. Acta* **53**, 1035–1040 (1989).
13. Hale, V. P. S., McSween, H. Y. Jr & McKay, G. Re-evaluation of intercumulus liquid composition and oxidation state for the Shergotty meteorite. *Geochim. Cosmochim. Acta* **63**, 1459–1470 (1999).
14. McKay, G., Mikouchi, T., Le, L., Schwandt, C. & Hashimoto, M. The Shergotty paradox: An experimental perspective on intercumulus melt compositions. *Lunar Planet. Sci. [CD-ROM]* **31** (2000).
15. McCoy, T. J. & Lofgren, G. E. Crystallization of the Zagami shergottite: An experimental study. *Earth Planet. Sci. Lett.* **173**, 397–411 (1999).
16. Anderson, D. J., Lindsley, D. H. & Davidson, P. M. QUILF: A Pascal program to assess equilibria among Fe-Mg-Mn-Ti oxides, pyroxenes, olivine, and quartz. *Comput. Geosci.* **19**, 1333–1350 (1993).
17. Hamilton, D. L., Burnham, C. W. & Osborn, E. F. The solubility of water and effects of oxygen fugacity and water content on crystallization in mafic magmas. *J. Petrol.* **5**, 21–39 (1964).
18. Sisson, T. W. & Grove, T. L. Experimental investigations of the role of H₂O in calc-alkaline differentiation and subduction zone magmatism. *Contrib. Mineral. Petrol.* **113**, 143–166 (1993).
19. Moore, G., Venneman, T. & Carmichael, I. S. E. An empirical model for the solubility of H₂O in magmas to 3 kilobars. *Am. Mineral.* **83**, 36–42 (1998).
20. Johnson, M. C., Rutherford, M. J. & Hess, P. C. Chassigny petrogenesis: Melt compositions, intensive parameters, and water contents of martian(?) magmas. *Geochim. Cosmochim. Acta* **55**, 349–366 (1991).
21. Miniti, M. M. & Rutherford, M. J. Genesis of the Mars Pathfinder “sulfur-free” rock from SNC parental liquids. *Geochim. Cosmochim. Acta* **64**, 2535–2547 (2000).
22. Wilson, L. & Head, J. W. Ascent and eruption of basaltic magma on the Earth and Moon. *J. Geophys. Res.* **86**, 2971–3001 (1981).
23. Mouginis-Mark, P. J., Wilson, L. & Zuber, M. T. in *Mars* (eds Kieffer, H. H., Jakosky, B. M., Snyder, C. W. & Matthews, M. S.) 424–452 (Univ. Arizona Press, Tucson, 1992).
24. Newman, S., Epstein, S. & Stolper, E. Water, carbon dioxide, and hydrogen isotopes in glasses from the ca. 1340 A. D. eruption of the Mono Craters, California: Constraints on degassing phenomena and initial volatile content. *J. Volcanol. Geotherm. Res.* **35**, 75–96 (1988).
25. Mustard, J. F., Murchie, S., Erard, S. & Sunshine, J. M. In situ compositions of Martian volcanics: Implications for the mantle. *J. Geophys. Res.* **102**, 25605–25615 (1997).
26. Bandfield, J. L., Hamilton, V. E. & Christensen, P. R. A global view of martian surface compositions from MGS-TES. *Science* **287**, 1626–1630 (2000).
27. Lodders, K. & Fegley, B. Jr An oxygen isotope model for the composition of Mars. *Icarus* **126**, 373–394 (1997).
28. Jones, J. H. Isotopic relationships among the shergottites, the nakhlites and Chassigny. *Proc. Lunar Planet. Sci. Conf.* **19**, 465–474 (1989).
29. Longhi, J. Complex magmatic processes on Mars: Inferences from the SNC meteorites. *Proc. Lunar Planet. Sci. Conf.* **21**, 695–709 (1991).
30. Herd, C. D. K. & Papike, J. J. Oxygen fugacity of the martian basalts from analysis of iron-titanium oxides: Implications for mantle-crust interaction on Mars. *Met. Planet. Sci.* **35**, A70 (2000).

Supplementary information is available on Nature's World-Wide Web site (<http://www.nature.com>) or as paper copy from the London editorial office of Nature.

Acknowledgements

This work was partly supported by NASA.

Correspondence and requests for materials should be addressed to H.Y.McS. (e-mail: mcsween@utk.edu).

Observation of coherent optical information storage in an atomic medium using halted light pulses

Chien Liu*†, Zachary Dutton*‡, Cyrus H. Behroozi*† & Lene Vestergaard Hau*†‡

*Rowland Institute for Science, 100 Edwin H. Land Boulevard, Cambridge, Massachusetts 02142, USA

†Division of Engineering and Applied Sciences, ‡Department of Physics, Harvard University, Cambridge, Massachusetts 02138, USA

Electromagnetically induced transparency^{1–3} is a quantum interference effect that permits the propagation of light through an otherwise opaque atomic medium; a ‘coupling’ laser is used to create the interference necessary to allow the transmission of resonant pulses from a ‘probe’ laser. This technique has been used^{4–6} to slow and spatially compress light pulses by seven orders of magnitude, resulting in their complete localization and containment within an atomic cloud⁴. Here we use electromagnetically induced transparency to bring laser pulses to a complete stop in a magnetically trapped, cold cloud of sodium atoms. Within the spatially localized pulse region, the atoms are in a superposition state determined by the amplitudes and phases of the coupling and probe laser fields. Upon sudden turn-off of the coupling laser, the compressed probe pulse is effectively stopped; coherent information initially contained in the laser fields is ‘frozen’ in the atomic medium for up to 1 ms. The coupling laser is turned back on at a later time and the probe pulse is regenerated: the stored coherence is read out and transferred back into the radiation field. We present a theoretical model that reveals that the system is self-adjusting to minimize dissipative loss during the ‘read’ and ‘write’ operations. We anticipate applications of this phenomenon for quantum information processing.

With the coupling and probe lasers used in the experiment, the atoms are accurately modelled as three-level atoms interacting with the two laser fields (Fig. 1a). Under perfect electromagnetically-induced transparency (EIT) conditions (two-photon resonance), a stationary eigenstate exists for the system of a three-level atom and resonant laser fields, where the atom is in a ‘dark’, coherent superposition of states |1> and |2>:

$$|D\rangle = \frac{\Omega_c|1\rangle - \Omega_p|2\rangle \exp[i(\mathbf{k}_p - \mathbf{k}_c) \cdot \mathbf{r} - i(\omega_p - \omega_c)t]}{\sqrt{\Omega_c^2 + \Omega_p^2}} \quad (1)$$

Here Ω_p and Ω_c are the Rabi frequencies, \mathbf{k}_p and \mathbf{k}_c the wavevectors, and ω_p and ω_c the optical angular frequencies of the probe and coupling lasers, respectively. The Rabi frequencies are defined as $\Omega_{p,c} \equiv e \mathbf{E}_{p,c} \cdot \mathbf{r}_{13,23} / \hbar$, where e is the electron charge, $\mathbf{E}_{p,c}$ are the slowly varying envelopes of probe and coupling field amplitudes, and $e \mathbf{r}_{13,23}$ are the electric dipole moments of the atomic transitions. The dark state does not couple to the radiatively decaying state |3>, which eliminates absorption of the laser fields^{1–3}.

Atoms are prepared (magnetically trapped) in a particular internal quantum state |1> (Fig. 1a). The atom cloud is first illuminated by a coupling laser, resonant with the |2>–|3> transition. With only the coupling laser on and all atoms in |1>, the system is in a dark state (equation (1) with $\Omega_p = 0$). A probe laser pulse, tuned to the |1>–|3> transition and co-propagating with the coupling laser, is subsequently sent through the atomic medium. Atoms within the pulse region are driven into the dark-state superposition of states |1> and |2>, determined by the ratio of the instantaneous Rabi frequencies of